Engineering Structures 234 (2021) 111868

Contents lists available at ScienceDirect

Engineering Structures

journal homepage: www.elsevier.com/locate/engstruct

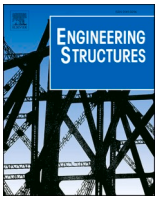

Numerical and analytical studies of ship deckhouse impact with steel and RC bridge girders

Yanyan Sha [a], Jørgen Amdahl [b], Cato Dørum [c,*]

[a] Department of Mechanical and Structural Engineering and Materials Science, University of Stavanger, Stavanger, Norway
[b] Centre for Autonomous Marine Operations and Systems, Department of Marine Technology, Norwegian University of Science and Technology, Trondheim, Norway
[c] Norwegian Public Roads Administration, Hamar, Norway

ARTICLE INFO

Keywords:
Ship collision
Bridge girder
Impact force
Collision energy
Analytical method

ABSTRACT

Bridges crossing navigable waterways are under the threat of accidental collisions from passing ships. However, previous research focus was mainly placed on ship collision with bridge substructures while ship-bridge superstructure collisions were largely ignored. In fact, superstructure collision accidents between bridge girders and ship deckhouses have occurred with increasing frequency in the past decade. Therefore, it is important to evaluate the bridge girder capacity against ship superstructure collisions in the design phase. In this paper, finite element models of a ship deckhouse and three types of bridge girders are established. Numerical simulations are conducted to investigate the response of the bridge girders under ship deckhouse collisions. The application and validity of the commonly adopted rigid body assumption of bridge girders are investigated. The results are compared with integrated collision simulations where both the striking deckhouse and the struck bridge girder are modelled as deformable bodies. The impact force, structural failure mode, and energy dissipation during the collision process are discussed. The effects of girder material and structural configuration are also discussed. Based on the numerically obtained failure mode of the ship deckhouse, an efficient analytical design approach for bridge girders against ship deckhouse impacts is proposed.

1. Introduction

Bridge structures crossing navigable channels are under the threat of accidental collisions from passing ships. Ship-bridge collisions can be categorised into two scenarios: 1) ship-bridge substructure collisions and 2) ship-bridge superstructure collisions. Extensive research efforts have been made in ship-bridge substructure collisions, i.e. ship/barge bow collisions with bridge piers, pile caps and pylons [1–11]. However, ship-bridge superstructure collisions have been ignored. In fact, many such accidents have been reported during the past decade [12]. For example, The Friesenbrücke Bridge, a 335 m long railway bridge in Germany, was crushed and destroyed by the cargo ship "Emsmoon" in 2015 [13] (see Fig. 1 (a)). This bridge was then completely demolished, and a new bridge was built to replace the damaged bridge. More recently in 2018, a tanker was pushed by strong winds and rammed into the connecting bridge of Kansai International Airport in Japan, and severely damaged part of the bridge girder [14] (see Fig. 1 (b)). Excessive damage also occurred in the ship, especially in the deckhouse as shown in Fig. 1 (c).

Given that ship-bridge collisions can have significant consequences, special attention should be paid to the collision design of bridge superstructures. Generally, three approaches can be used for ship-bridge collision analysis, i.e. experimental tests, numerical simulations, and empirical formulae/charts.

1) Experimental tests

Experimental testing is the most direct method to obtain the impact load and the associated structural damage during the collision. However, due to the financial costs, labour efforts, and site limitations, reports of collision tests are quite limited in the literature. Minorsky [15] examined actual ship-ship collision events and proposed a linear relationship between the volume of the deformed material and the absorbed impact energy. The empirical formula accurately represents the energy-volume relationship for high energy cases. However, it is not appropriate for low-energy collision cases where large scatter of the results occurs [16]. Later, Woisin [17] conducted a number of high-energy ship collision tests and found that the equivalent static impact force of a large

* Corresponding author.
E-mail address: yanyan.sha@uis.no (C. Dørum).

https://doi.org/10.1016/j.engstruct.2021.111868
Received 19 May 2020; Received in revised form 3 November 2020; Accepted 4 January 2021
Available online 1 March 2021

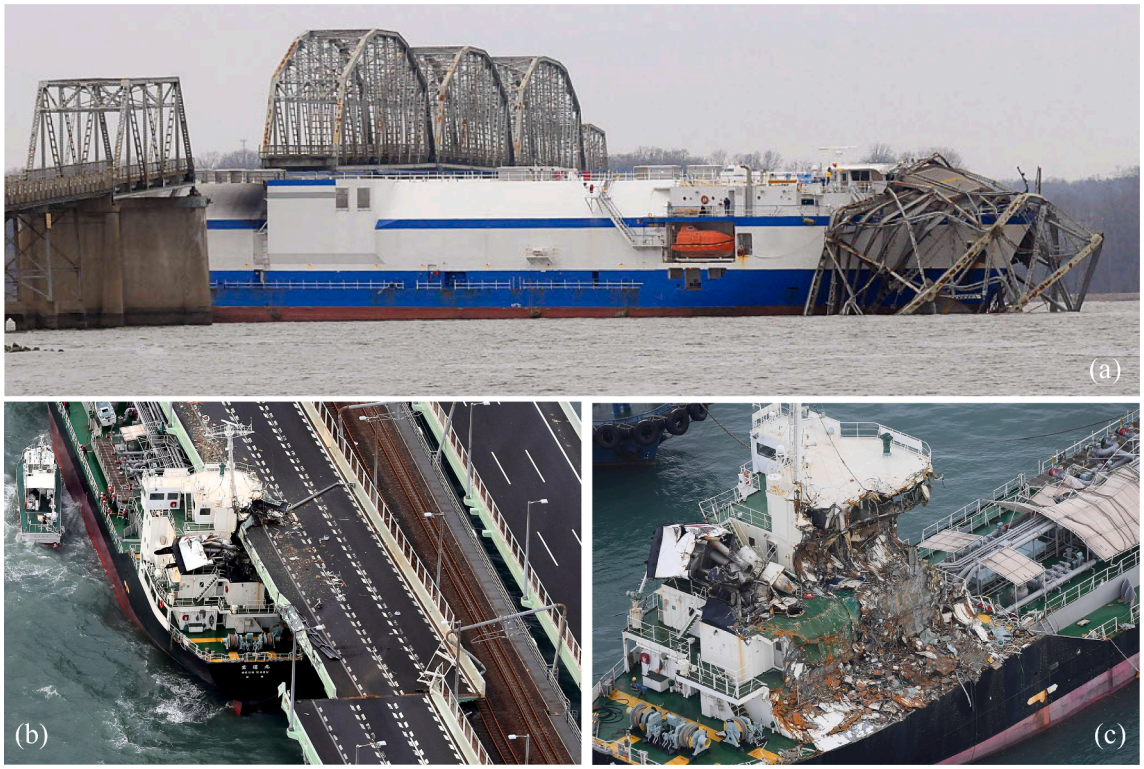

Fig. 1. (a) The Friesenbrücke Bridge girder destroyed by a cargo ship [13], (b) Kansai International Airport connecting bridge collide by a tanker, and (c) damage of the tanker [14].

ship against a rigid wall is proportional to the square root of the deadweight tonnage (DWT) of the ship [18]. Most of the previous experimental investigations were primarily conducted for ship-ship collisions. For ship-bridge collisions, almost no full-scale collision tests have been performed. Consolazio et al. [19] conducted barge collision tests on an abandoned bridge pier in 2002. However, given the test barge has much smaller DWT and bow dimensions compared with seagoing ships, the research findings cannot be directly applied to ship-bridge collisions. Moreover, the collision tests were only conducted for bridge substructures, i.e., bridge piers, supporting piles, and pile caps. No investigations of bridge superstructure collisions were carried out.

2) Numerical simulations

Numerical methods have been widely utilized in predicting the impact force, structural damage, and energy dissipation during ship collisions. However, most of the previous studies focused on ship-ship collisions [16,20–22], ship-offshore structure collisions [23–26], and ship-bridge substructure collisions [1,5,8,27–30]. Very limited numerical investigations can be found for ship-bridge superstructure collisions. Sha and Amdahl [12,31] reported a case study of cruise ship forecastle collision with a steel floating bridge girder. Local structural damage and global bridge response were identified and a girder strengthening technique was proposed. However, their work was limited to ship forecastle collision and the considered impact scenarios are limited while the variations of bridge girder geometry and material were not reported.

3) Empirical formulae/charts

Empirical formulae have been used in many design codes and guidelines owing to its simplicity. An equivalent static load is commonly assumed for the ship collision load in the design of bridge structures. Both Eurocode [32] and AASHTO (American Association of State Highway and Transportation Officials) code [33] suggest using an equivalent static load to represent the ship collision load based on the impact velocity and ship DWT. However, using equivalent static loads in design neglects the dynamic effects during the collision. Moreover, the proposed equivalent static load varies significantly from code to code [2].

Eurocode provides only an equation for estimating the ship collision force on bridge substructures while no recommendation is given for ship-bridge superstructure collisions. AASHTO advises calculating ship-bridge superstructure impact load by multiplying the ship-bridge substructure impact force P_s with a reduction factor. It should be noted that two reduction factors are proposed to account for ship deckhouse (R_{DH}) and ship forecastles (R_{BH}) collisions respectively.

$$P_s = 0.12\sqrt{DWT} \cdot V \tag{1}$$

$$P_{DH} = (R_{DH})(P_s) \tag{2}$$

$$P_{BH} = (R_{BH})(P_s) \tag{3}$$

where DWT is the deadweight tonnage of the vessel in tons and V is the vessel impact speed in m/s.

P_{DH} is the ship deckhouse impact load on bridge superstructures. The reduction factor $R_{DH} = 0.1$ for ships larger than 100,000 DWT and $R_{DH} = 0.2 - 0.1\left(\frac{DWT}{100000}\right)$ for ships smaller than 100,000 DWT.

P_{BH} is the ship bow (forecastle) impact load on bridge superstructures and R_{BH} is the ratio of exposed superstructure depth to the total bow depth.

Pedersen et al. [34] pointed out that the deckhouse impact force depends highly on the contact height which is directly related to the girder geometry. Based on the design investigation of the Great Belt Bridge project, it is recommended that the design deckhouse impact loads be calculated depending on the size of the contact area, i.e. the product of the contact height and the breadth of the deckhouse. The

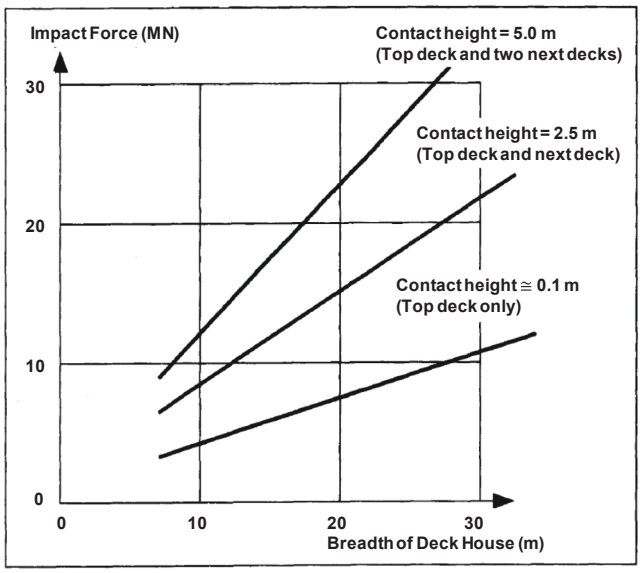

Fig. 2. Impact force chart for deckhouse collision with bridge superstructures [34].

deckhouse impact loads on the bridge superstructures should be obtained from the loads required to deform the structural elements of the deckhouse. The relationship between the impact force and the contact area is illustrated in Fig. 2. It is noted that the chart is developed based on relatively small vessels and the suggested impact force has included the probability of angled impacts.

The empirical formulae and design charts are easy to use in the preliminary design phase due to their simplicity. However, these empirical formulae and charts only take into account the principle ship characteristics, i.e. ship DWT and impact velocity, girder height, and deckhouse breadth while the effects of impact location, girder geometry, girder strength, and girder material are ignored. To have a comprehensive understanding of the bridge girder resistance to ship deckhouse impacts, the influence of these parameters should be further investigated.

1.1. Objectives of this study

The objective of the present study is to investigate the behaviour of various bridge girders subjected to ship deckhouse collisions accounting for ship-bridge interactions. In this work, finite element (FE) models of a ship deckhouse and three types of bridge girders are established based on technical drawings. Numerical simulations of the collision between the ship deckhouse and the bridge girders are conducted. First, the validity of a rigid girder assumption for simulation of a deckhouse-girder collision is discussed. Next, the demand for energy dissipation and associated structural damage are investigated when both the ship deckhouse and the bridge girder are assumed deformable (integrated analysis). The following collision scenarios are investigated:

- A rigid wedge indenter impacting with a deformable ship deckhouse.
- Two rigid trapezoidal prism indenters with different configurations impacting with a deformable ship deckhouse.
- Deformable ship deckhouse collision with two types of deformable steel girders.
- Deformable ship deckhouse collision with a deformable reinforced concrete girder.

Based on the numerical simulation results, the validity and limitations of the empirical formulae and design charts are discussed. An analytical approach for estimation of the deckhouse-girder impact force is proposed based on the failure mechanism of structural components observed in the numerical simulations. It should be noted that this study focused on local structural resistance and deformation. The structural deformation and energy dissipation are thus referred to local response only. The interaction between ship motion and bridge girder vibration are not considered in this study. The global response of bridges under ship collisions can dissipate a large amount of the total collision energy, especially for large-span cable-stayed/suspension bridges and floating bridges [31,35]. This energy distribution between local structural deformation and global bridge vibrations varies significantly depending on the collision scenario and structural configurations. Extensive further studies on global bridge motion and local–global interactions are required for a complete understanding of the overall collision response.

2. Finite element models

2.1. Ship deckhouse model

A ship deckhouse model is developed for a container ship with a total length of 166 m and a beam width of 22.5 m as shown in Fig. 3. The structural components in the ship deckhouse were modelled in detail to accurately represent the structural stiffness as only the deckhouse is expected to be in direct contact with the bridge girder. The ship body was simply modelled by very coarse rigid shell elements to illustrate the shape and the dimension of the ship. As shown in Fig. 3 (b), the deckhouse panels, internal decks, girders and stiffeners were modelled with four-node shell elements. The plate thickness of the deckhouse and internal structures varies from 7 mm to 18 mm. A mesh size of 100 mm was generally used. The main dimensions of the ship including the

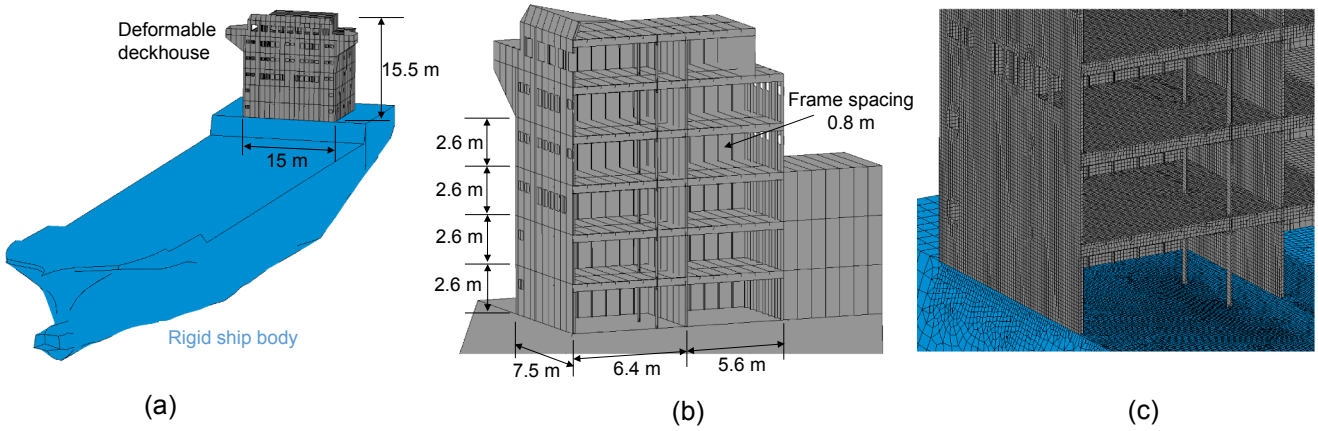

Fig. 3. (a) Container ship model, (b) detailed deckhouse modelling, and (c) mesh illustration.

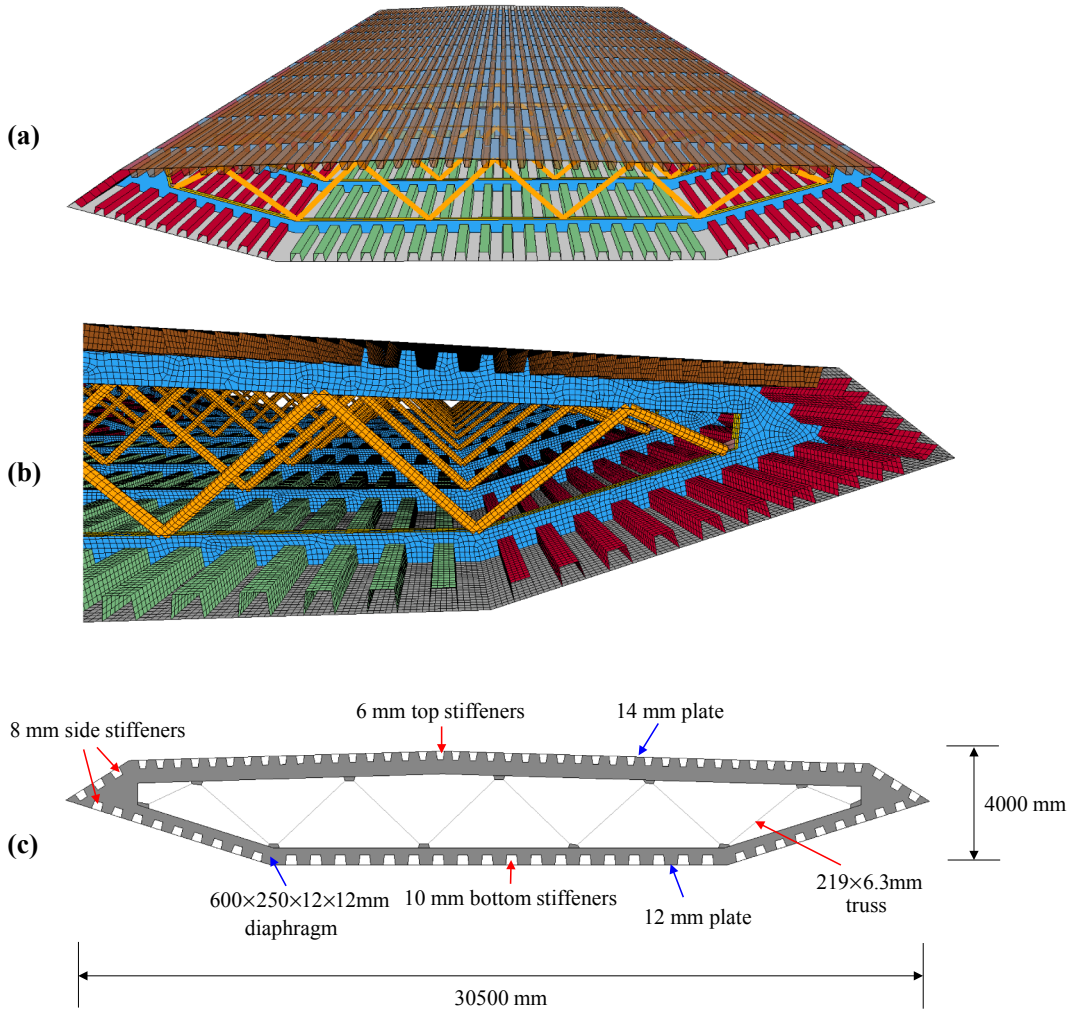

Fig. 4. FE model of the steel bridge Girder 1.

deckhouse are illustrated in Fig. 3.

2.2. Girder models

Three bridge girder prototypes as shown in Figs. 4-6 are selected in this study.

Girder 1 and Girder 2 as shown in Figs. 4 and 5 are two typical steel girders. These two girders have similar geometry and plate thickness for most of the structural components. A notable difference lies in the design of the girder edges. Girder 1 (Fig. 4) has an integrated design throughout the whole cross-section. The edge plate is supported by transverse diaphragms and continuously connected to the top and bottom girder panels. Girder 2 (Fig. 5) has external wind guide vanes for improving the aerodynamic performance of the girder which are hinged to the two thick (35 mm) vertical edge plates. The wind guide vanes are fabricated with thin (5 mm), unstiffened plates and thus have a very small contribution to the structural strength. Detailed dimensions and thicknesses of the two girders are illustrated in Figs. 4 and 5.

Girder 3 as shown in Fig. 6 is one of the twin reinforced concrete bridge girders. Discrete modelling technique applies to the concrete and the steel reinforcements [7,8]. The concrete was modelled by eight-node solid elements while the longitudinal and transverse steel reinforcements with a diameter of 20 mm were modelled with beam elements. The perfect bond assumption was adopted for the connection between the steel reinforcement and the concrete in this study [8]. This was achieved by sharing all nodes of the beam elements with the solid elements.

2.3. Material modelling

For the steel material in the ship and the steel bridge girders, a power-law hardening model [36] was used. The material was assumed to have isotropic plastic properties and modelled using plane stress J2 flow theory. Material failure was considered by incorporating the Rice-Tracey-Cockcroft-Latham (RTCL) damage criterion [36]. The element size for the FE model is around 5 to 10 times of the plate thickness. To get a better prediction of strain and fracture, the damage criterion is scaled according to mesh size. The ship deckhouse is fabricated in mild steel. The yield stress is set to 275 MPa to reflect more correctly the expected strength. The steel girder which was constructed in high strength steel with a characteristic yield strength of 420 MPa. Detailed parameters for the material are tabulated in Table 1.

The extended Karagozian & Case (K&C) model (MAT_CONCRETE_DAMAGE_REL3) which takes into account the concrete damage in form of failure surfaces was used in the modelling of the concrete bridge girder. This model is widely employed to simulate the dynamic behaviour of concrete material including plasticity and damage softening after failure. The concrete in the pontoon has a compressive strength of 60 MPa and the failure strain was set to 0.1 [8]. The elastic–plastic material model MAT_PIECEWISE_LINEAR_PLASTICITY (MAT_24) was employed to model the steel reinforcements in the RC bridge girder. It is a cost-effective model and includes isotropic and kinematic hardening

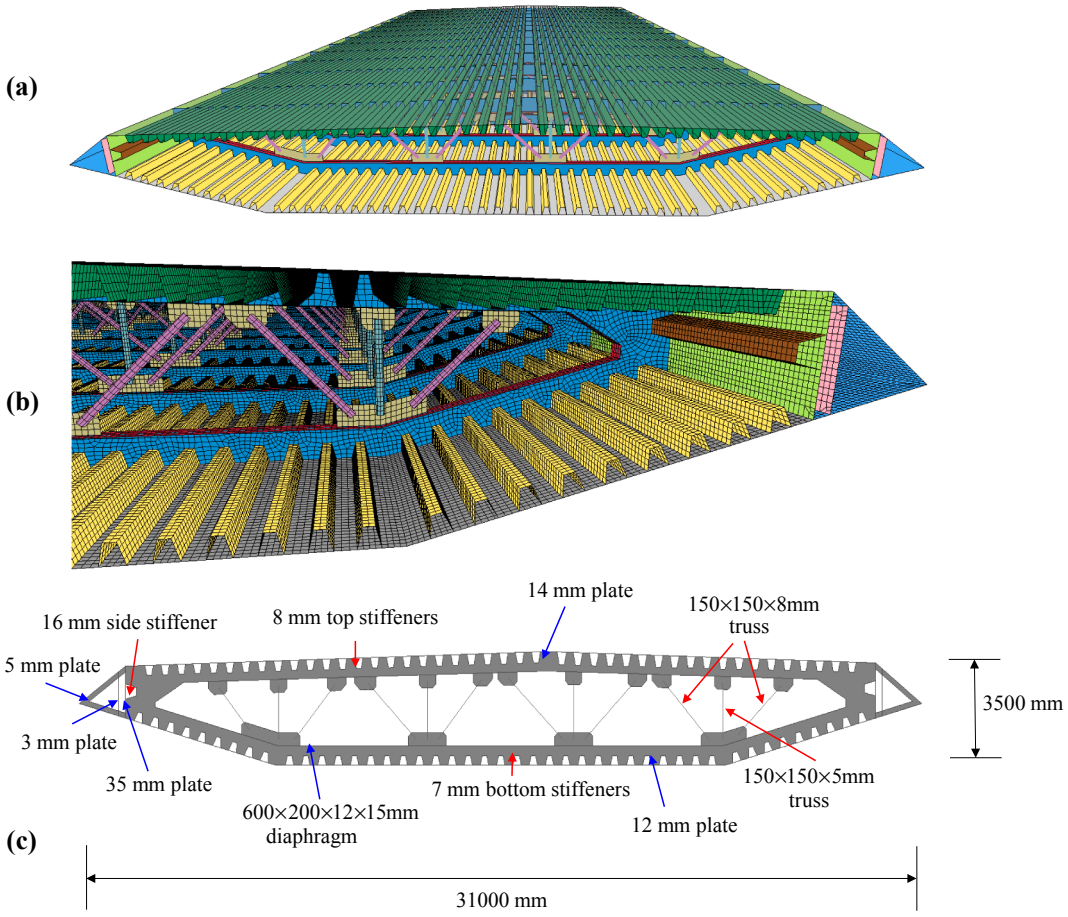

Fig. 5. FE model of the steel bridge Girder 2.

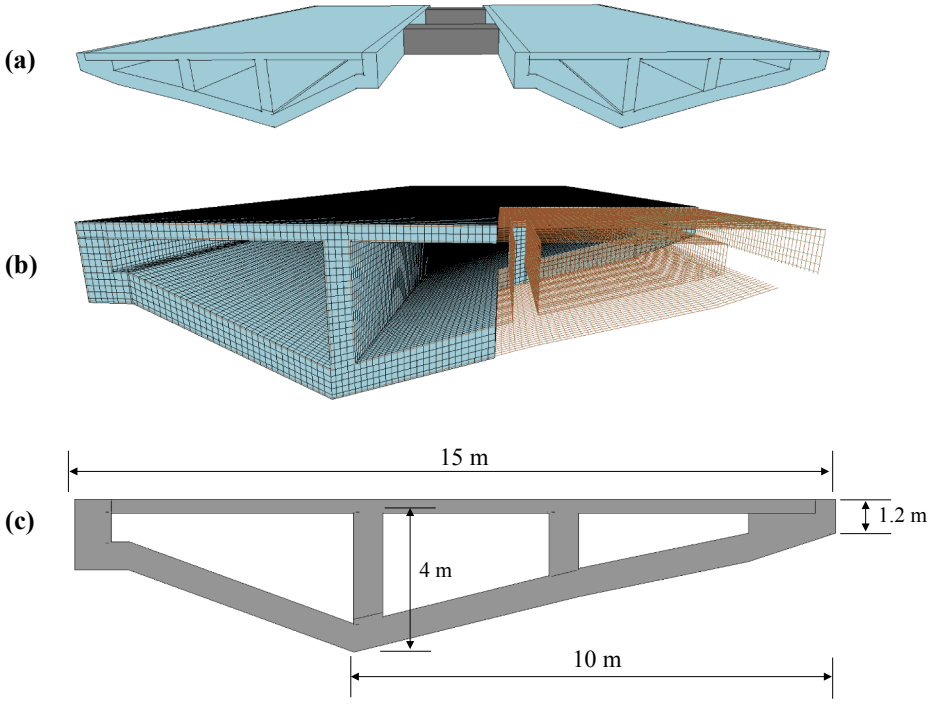

Fig. 6. FE model of the reinforced concrete bridge girder (Girder 3).

Table 1
Steel and concrete material parameters in the ship deckhouse and bridge girders.

Component	Material	Parameter	Value
Ship deckhouse	Steel	Density	7890 kg/m^3
		Young's modulus	210 GPa
		Poisson's ratio	0.3
		Yield stress	275 MPa
		Strength index	740 MPa
		Strain index	0.24
Steel girder	Steel	Density	7850 kg/m^3
		Young's modulus	210 GPa
		Poisson's ratio	0.3
		Yield stress	420 MPa
		Strength index	863 MPa
		Strain index	0.15
RC girder	Concrete	Density	2400 kg/m^3
		Poisson's ratio	0.2
		Compressive strength	60 MPa
		Failure strain	0.1
	Steel (Reinforcements)	Density	7850 kg/m^3
		Poisson's ratio	0.3
		Young's modulus	2.1E11
		Yield stress	275 MPa
		Failure strain	0.35

plasticity. The steel reinforcement has a yield stress of 275 MPa.

The concrete and steel materials are strain rate dependent when subjected to impact loads. At high strain rates, e.g. in the blast and projectile simulations, the strength of concrete and steel materials can be significantly enhanced. However, for low-velocity impacts such as ship collisions, the influence of strain rate remains debatable although many research efforts have been devoted [37–39]. In this study, the strain rate effect was neglected. The main reason is that the strain rate effect is relatively small in the present case and is rather uncertain and challenging to analyse properly [40]. It is normally conservative to neglect it for the struck bridge but is unconservative for the crushing force of the striking ship deckhouse. It is also likely that the two effects may cancel each other to some extent [7].

2.4. Boundary conditions

In the simulations, the bridge girders are fixed at both ends in the longitudinal direction as shown in Fig. 7. The rigid ship body is prescribed with a constant velocity of 10 m/s in the transverse direction of the bridge girder. No extra boundary condition is applied to the ship deckhouse.

3. Deformable deckhouse impacted by rigid indenters

In ship-ship collision simulations, striking ships are commonly treated as rigid bodies, since the striking ship bows are normally stronger than the side structures of the stuck ships. Similarly, in a deckhouse-girder collision simulation, the relatively stronger bridge girders are first assumed as rigid bodies while the ship deckhouse is considered as a deformable body. Three rigid indenters are constructed to reflect the edge shape of the three bridge girders in Figs. 4-6. The wedge-shaped indenter as shown in Fig. 8 (a) is representative for the steel bridge girder with a sharp integrated edge (Girder 1). For Girder 2, a rigid indenter based on the overall geometry of the girder will significantly underestimate the impact demand. This is because the wind guide vanes are very weak and have almost no contribution to the structural strength. Hence, the wind guide vanes are excluded as shown

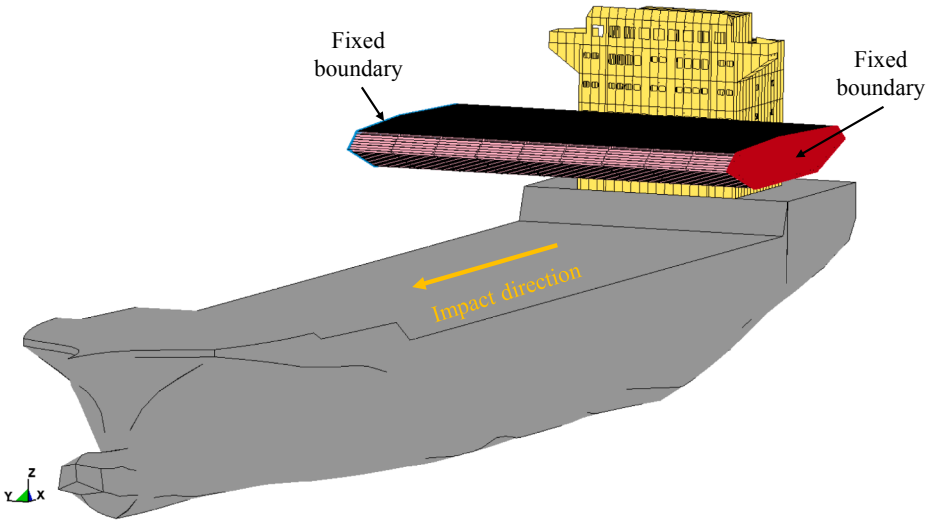

Fig. 7. Collision setup for steel bridge girder 1.

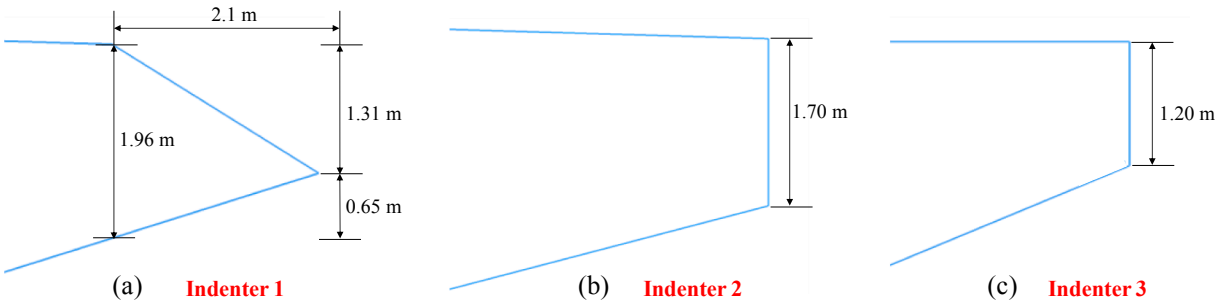

Fig. 8. Geometries of the two rigid indenters, (a) wedge shape indenter 1, (b) trapezoidal prism shape indenter 2, and (c) trapezoidal prism shape indenter 3.

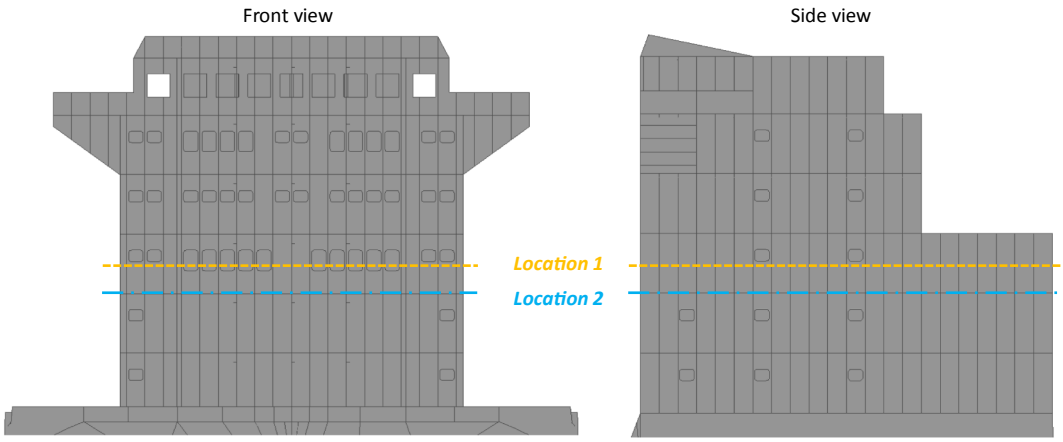

Fig. 9. Girder impact location on the ship deckhouse.

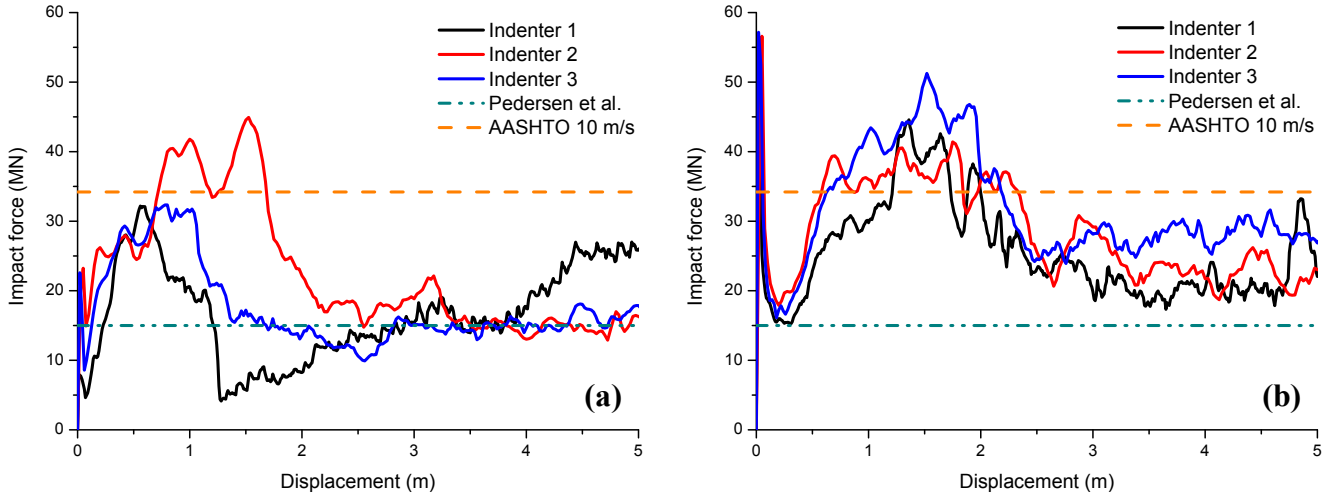

Fig. 10. Force-displacement curves of the ship deckhouse subjected to the impact of three rigid indenters, (a) impact at Location 1, and (b) impact at Location 2.

in Fig. 8 (b). For the reinforced concrete bridge girder (Girder 3), a trapezoidal prism indenter as shown in Fig. 8 (c) is used.

In a real collision incident, the vertical impact location on the ship deckhouse may vary due to ship loading conditions (draft and trim), tidal variations and any wave-induced motions. As ship deckhouses have relatively strong horizontal decks, the collision response will be different for impacts between two decks or on deck level. Therefore, as shown in Fig. 9., two typical collision scenarios are considered: impact in the middle of two decks (Location 1) and impact at deck level (Location 2). Since the bridge girder model is considerably longer than the ship

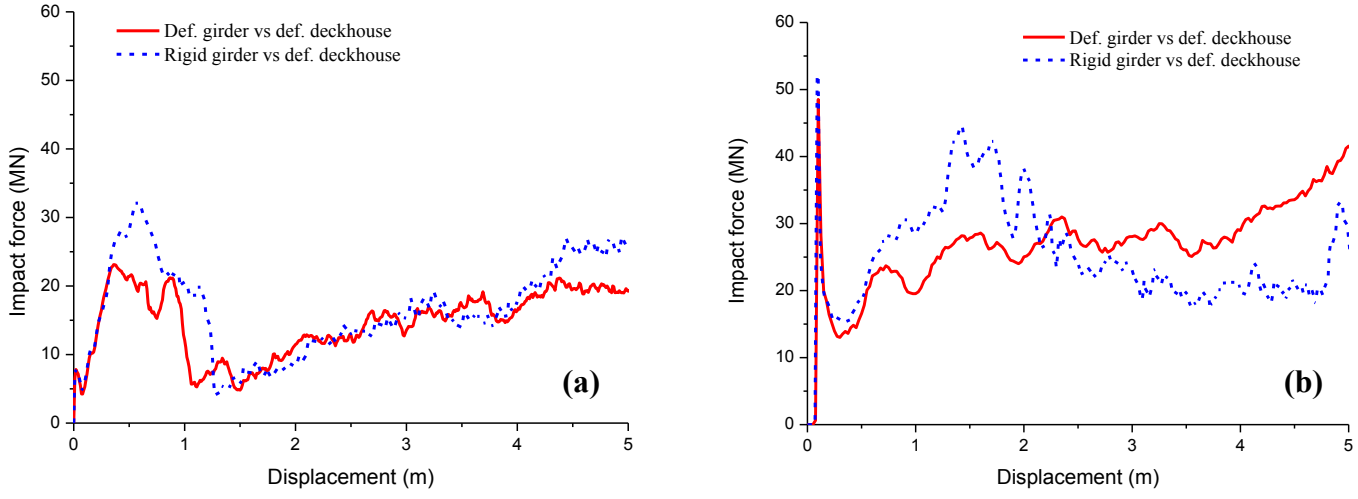

Fig. 11. Force-displacement curves of Girder 1 for the collision at (a) location 1 and (b) location 2.

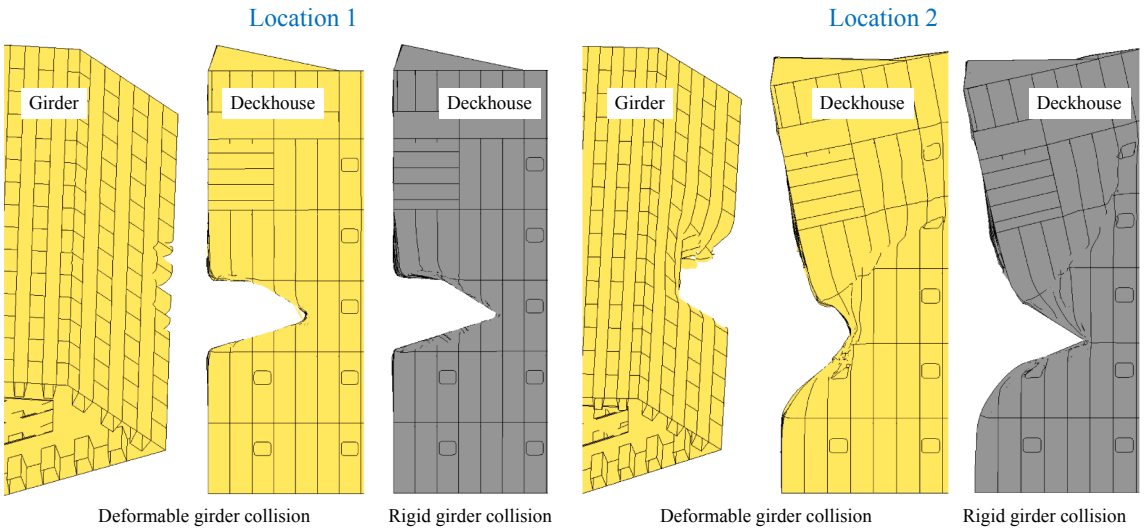

Fig. 12. Deckhouse deformation when impacted by Girder 1.

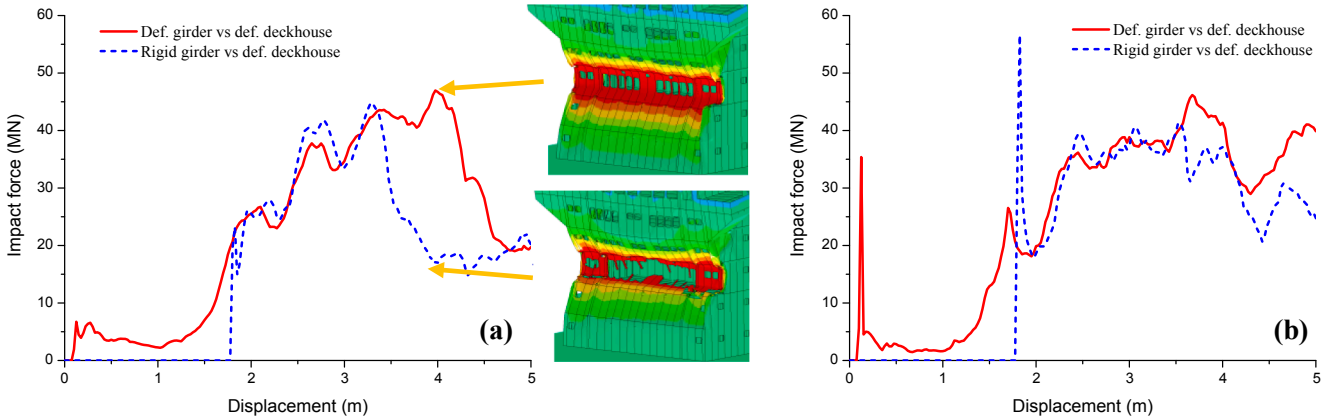

Fig. 13. Force-displacement curves of Girder 2 for the collision at (a) location 1 and (b) location 2.

deckhouse, the variation of horizontal impact location does not have any effect on the collision response and is thus neglected. In both cases, the ship hits normal to the bridge girder.

The force–displacement curves of the ship deckhouse impact with three rigid indenters are displayed in Fig. 10. The impact forces calculated from the equations suggested by AASHTO [33] and the chart proposed by Pedersen et al. [34] are also plotted in the same figures for comparison.

For impact at Location 1, the geometry of the indenter strongly

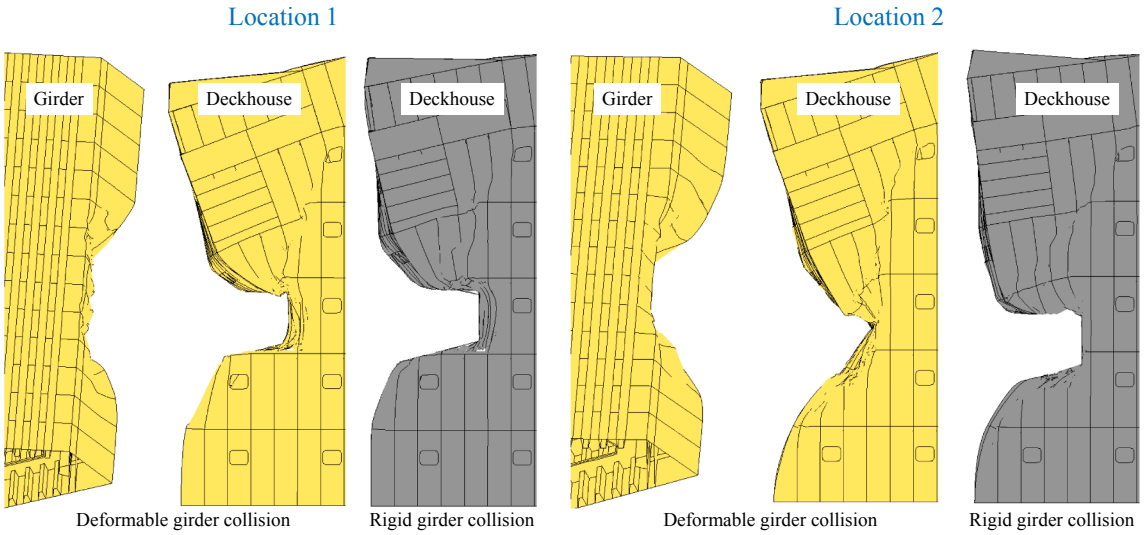

Fig. 14. Deckhouse deformation when impacted by Girder 2.

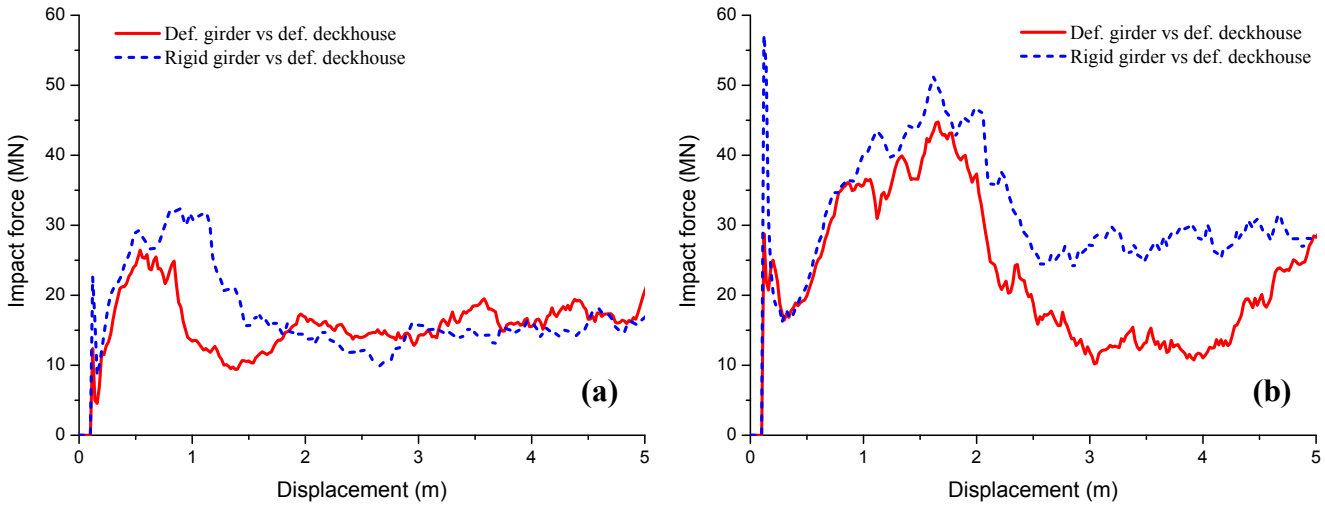

Fig. 15. Force-displacement curves of Girder 3 for the collision at (a) location 1 and (b) location 2.

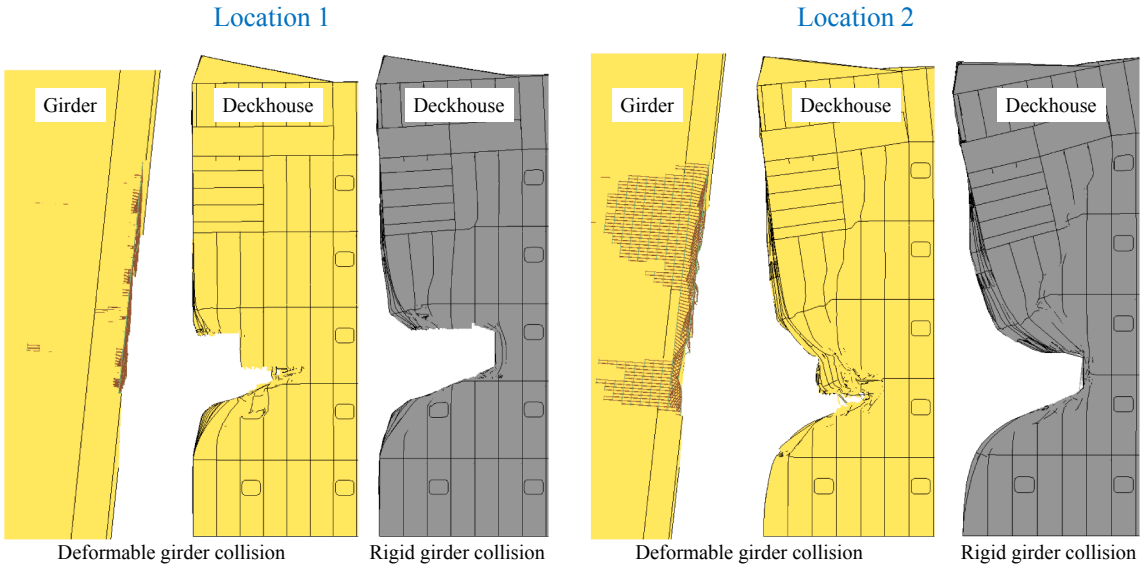

Fig. 16. Deckhouse deformation when impacted by Girder 3.

influences the plastic deformation and failure mechanism of the deckhouse. The first peak represents the local resistance of the deckhouse front panel and is dominated by the contact area between the indenter and the panel. Hence, a wedge shape indenter has a much smaller first peak force than the trapezoidal prism indenters. The subsequent slope of the force-indentation curve is almost the same for the three indenters as it is dominated by the membrane force of the stiffened front panel in the deckhouse. This slope is maintained until excessive plastic deformation occurs in the front plate and fracture starts to develop. The dramatic drop of the force–displacement curve indicates initiation of fracture in the front panel. When the deckhouse is crushed by the trapezoidal prism Indenters 2 and 3, the flat edge of the indenter quickly engages the adjacent plates in the decks above and below. This results in a higher impact force for the prism-shaped indenters than for the wedge shape Indenter 1. For the indenter with a height of 1.2 m (Indenter 3), the impact force increases to 32 MN with a delayed fracture initiation at a displacement of around 1.1 m. For the indenter with a height of 1.7 m (Indenter 2), the maximum impact force is 45 MN at 1.7 m displacement. After a complete plate rupture, the impact force has contributions only from the resistance of the vertical side plates and therefore it is in a similar range for the three indenters.

For impact at Location 2, an instantaneous higher peak force occurs regardless of the indenter shape. This is due to the crushing of the horizontal deck in the ship deckhouse. However, this large peak only lasts for a very short time and diminishes as the deck experiences continuous folding damage when the indentation continues. The force level for Location 2 is generally much higher compared to that for Location 1 during the whole indentation process. The force–displacement curves are generally comparable for the three indenters.

The impact force suggested by AASHTO (see Eqs (1) and (2)) changes linearly with respect to the impact velocity. For an impact velocity of 10 m/s, the AASHTO code yields a larger impact force than that for Indenter 1 and 3 when impacting at Location 1. For the other impact scenarios, the code tends to give a lower force than the maximum impact force as shown in Fig. 10. Nevertheless, the energy absorbed by assuming a constant force is close to the simulations. As the equivalent static impact force is calculated based solely on ship DWT and impact velocity, it cannot account for the change of impact location, geometry, material and strength of the ship deckhouse and bridge girder, and the temporal variation during the collision process.

The design chart proposed by Pedersen et al. is based on small vessels with the breadth of the deckhouse and the girder height as shown in

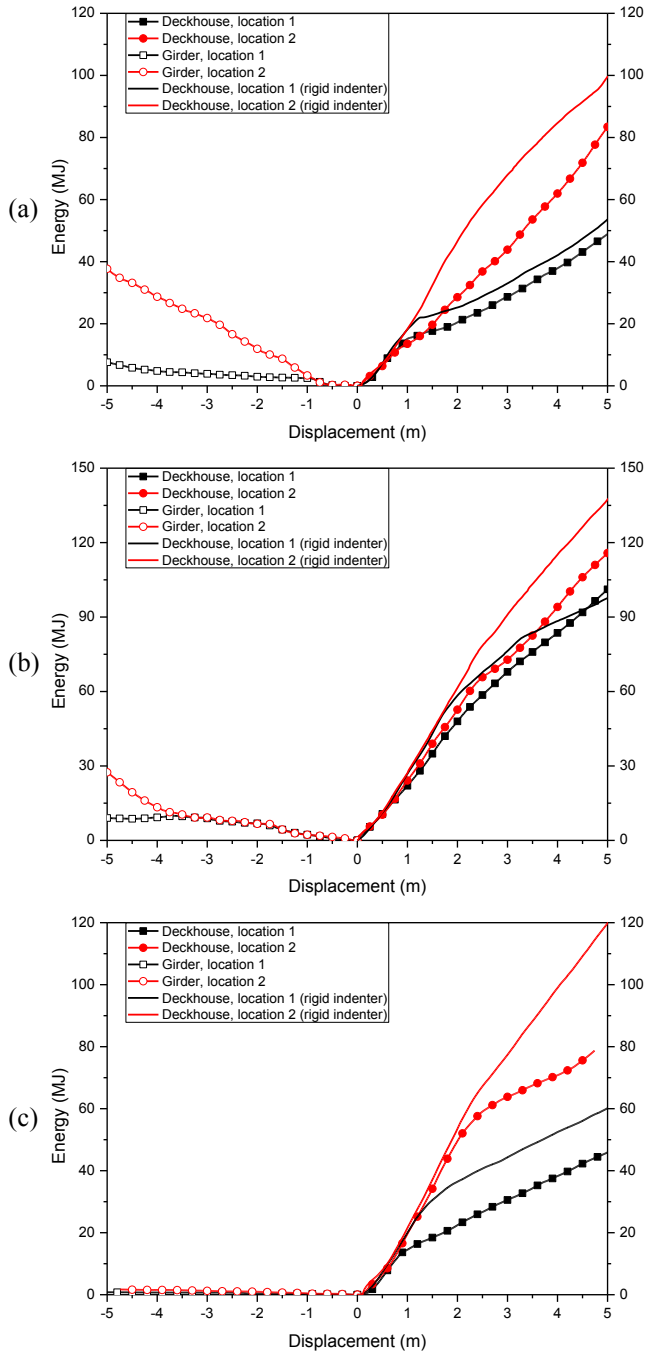

Fig. 17. Energy dissipation curves. (a) Steel Girder 1, (b) steel Girder 2, and (3) RC Girder 3.

Fig. 2. The impact forces from the design chart are generally smaller than the impact force obtained from the numerical simulations. This may be attributed to the fact that the design chart has taken into account of the collision angle. For an oblique impact, the contact area is smaller than the head-on impact, and thus the impact force will also be smaller.

4. Integrated collision simulations

Interactions between the striking and the struck structures can have a significant influence on the collision response of both structures [25]. In this section, integrated numerical simulations with deformable ship deckhouse and bridge girders are conducted. The impact force and structural damage are compared with the simulations using rigid indenters. The validity of the rigid girder assumption is then discussed. For all cases, the displacement means the prescribed motion of the ship, which accounts for the deformations of both the ship deckhouse and the bridge girder.

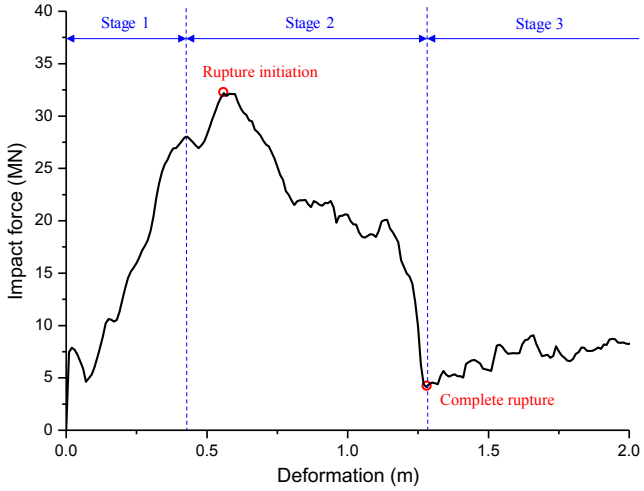

Fig. 18. Force-deformation curve of the collision and the corresponding deckhouse deformations for the three impact stages [42].

4.1. Collision with the steel girder 1

For impact at Location 1, the force level for deckhouse collision with the deformable girder and the rigid girder is almost identical until 0.3 m displacement as shown in Fig. 11 (a). Then, the impact force starts to decrease as fracture initiates in the deckhouse front panel in the rigid girder case. In the integrated analysis, the fracture initiation is delayed because of slight deformation of the girder and associated "softening" of the structure at the contacted area. The "plateau" in the force–displacement curve is thus wider as the deformation of the girder prolongs the interaction process. The impact forces of the two cases are generally comparable and the deckhouse damage is also similar as shown in Fig. 12.

For impact at Location 2 where the girder impacts at the deck level of the deckhouse, the impact forces are generally higher than those obtained for Location 1. The force in the rigid girder case is higher than that in the integrated analysis until 2.2 m displacement. This is because more structural components in the deckhouse are engaged in the collision as shown in Fig. 12. Later, the impact force in the integrated analysis increases as the deformable girder undergoes deformations that result in a larger contact area. Note that in both cases the deckhouse is "pulled down" significantly, thus limiting the development of membrane forces.

4.2. Collision with the steel girder 2

For impact at location 1, the force–displacement curve for the deformable Girder 2 is quite different from that of Girder 1. The impact is about 5 MN until 1.5 m ship displacement and is due to the crushing of the wind guide vanes as shown in Fig. 13. When they are completely crushed, the penetration of the deckhouse starts.

The force attains a local peak of 27 MN at 2 m displacement when the front deckhouse panel fractures as shown in Fig. 14. After intermediate unloading, the force increases again as the bridge girder deforms the two adjacent decks. The impact force reaches its maximum when the front section of the deckhouse is pulled down as shown in Fig. 14. The rigid indenter without the shape edge generally has a good estimation of the impact force. A major difference occurs when the ship displacement is 3.5–4.5 m. This is because when the girder is deformable, the

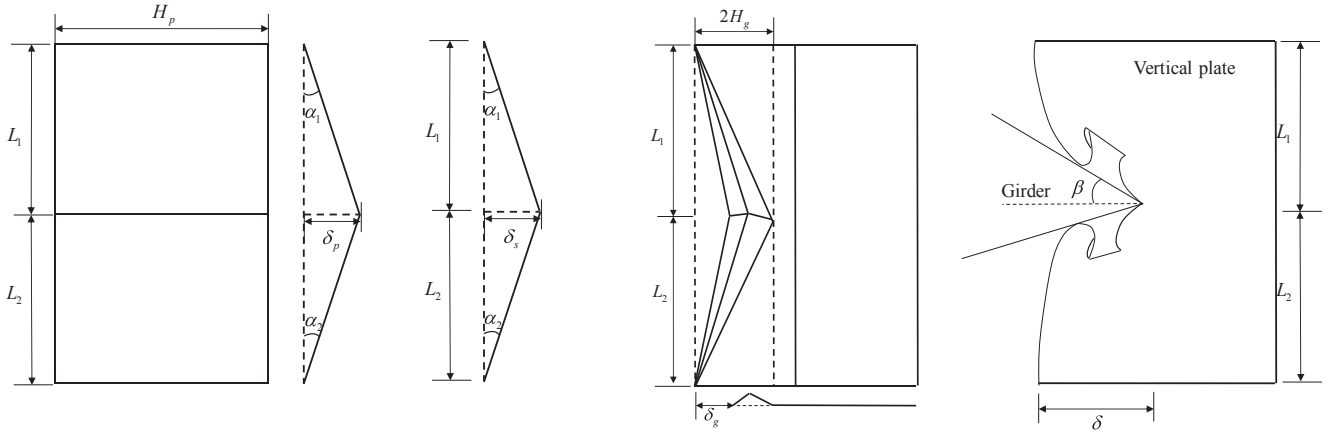

Fig. 19. The failure mechanism for (a) the front panel, (b) stiffener, (c) side panel folding, and (d) side panel tearing subjected to the impact of shape edge indenters.

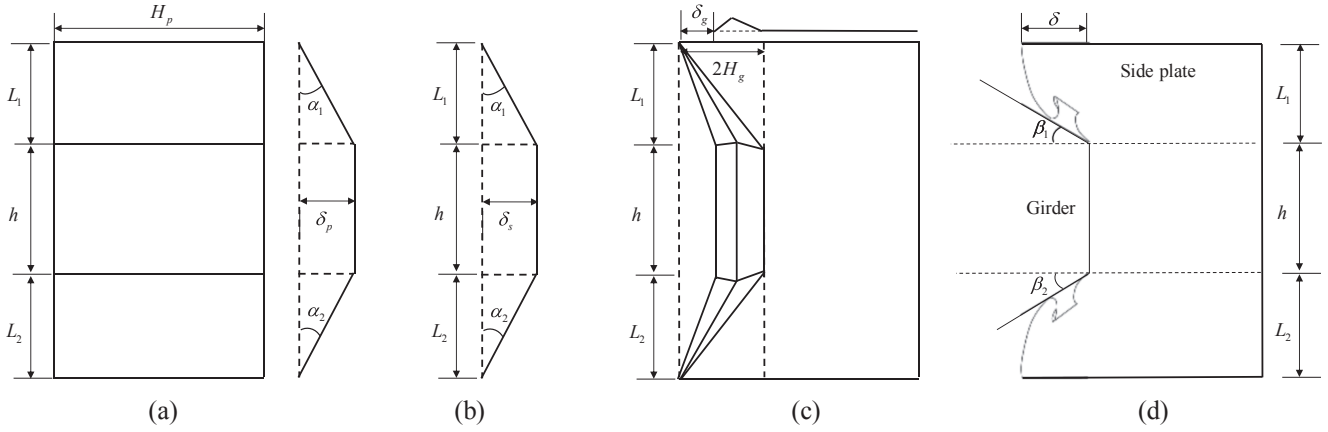

Fig. 20. The failure mechanism for (a) the front panel, (b) stiffener, (c) side panel folding, and (d) side panel tearing subjected to the impact of flat edge indenters.

deformation of the girder will result in a larger contact area. This increase of contact area leads to a redistribution of membrane forces to the adjacent panels and thus postponed the fracture initiation in the deckhouse front panel. Meanwhile, the rigid girder induces an earlier fracture in the deckhouse as shown in Fig. 13 (a).

For impact at location 2, the force–displacement curves obtained with a rigid girder and a deformable girder are quite similar. In the integrated analysis, the girder starts to deform after 3.5 m displacement and thus creating a larger contact area in the late stages. The deckhouse damage is also more severe compared to the rigid girder case as shown in Fig. 14.

4.3. Collision with the RC girder 3

For ship impacts with concrete structures, the energy absorption is commonly assumed to take place in the ship [24]. The energy dissipated by the concrete structure is considered negligible and thus it can be assumed to be rigid. This saves modelling and computational efforts. However, the concrete structures may be subject to high local pressure at certain instances during the impact period which may cause crushing, flexural or punching shear failure [7]. Hence, collision simulations with a deformable RC girder, i.e. integrated analyses, should be conducted.

Fig. 15 shows the peak forces are higher in the rigid girder cases than in the deformable girder cases. This attributes to the crushing failure of the concrete cover at the girder edge which releases the impact force in the integrated analysis as shown in Fig. 16. It should be noted that this response is transient in nature and thus does not have a considerable influence on the overall collision response as can be observed from the force–displacement curves. For both impact locations, the maximum force in the rigid girder cases is about 10%-20% higher.

4.4. Discussions on structural damage and energy dissipation

For deckhouse impact with steel Girder 1, the energy dissipation curves are shown in Fig. 17 (a). The deckhouse dissipates the majority of the collision energy for both impact locations. Both the girder and the deckhouse dissipate more energy when impact occurs at the deck level (Location 2). A rigid girder assumption gives a decent estimation of the energy dissipation.

The energy dissipations for deckhouse impact with steel Girder 2 are shown in Fig. 17 (b). It should be noted that the energy dissipation of the wind guide vanes in the bridge girder is very small and is thus neglected. It can be observed that the energy dissipation is insensitive to the impact location in the integrated analyses. Rigid girder assumption yields a reasonable estimation of the energy dissipation.

For integrated analysis of deckhouse impact with RC Girder 3, major damage occurs in the ship deckhouse while the RC girder only endures minor surface spalling in the concrete cover. As shown in Fig. 17 (c), the ship deckhouse absorbs more than 90% of the total collision energy. The estimation of energy dissipation in the ship deckhouse is also found to be conservative when the deckhouse is impacted by a rigid girder.

Therefore, the girder geometry and relative impact location can have a significant influence on the impact force, and consequently on the energy dissipation. The rigid girder assumption generally gives an accurate yet conservative estimation on the impact demand and energy dissipation. Therefore, the bridge girders may be assumed to be rigid in

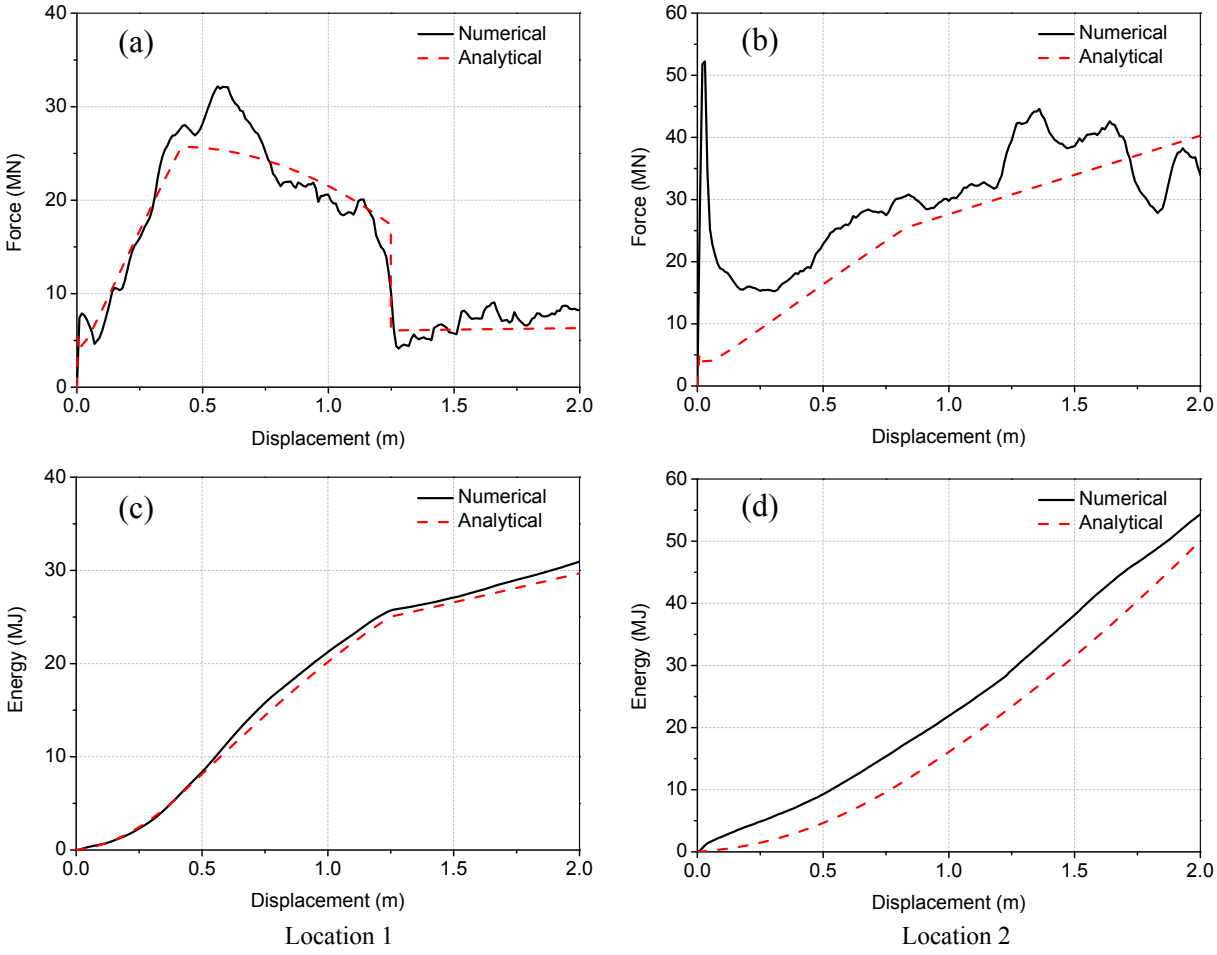

Fig. 21. Comparison between numerical and analytical results for collision with Girder 1. (a) Force at Location 1, (b) force at Location 2, (c) energy at Location 1, (d) energy at Location 2.

the early design phase to save modelling and computational efforts.

4.5. Discussions on the existing codes

The AASHTO code suggested using an equivalent static impact force in design. This force is calculated based only on the striking ship's displacement and impact velocity as described in Eqs (1) and (2). For the collision scenarios investigated in the current study, the code yields realistic impact forces in the sense that the average force levels agree well with the simulations. However, the equivalent forces obtained from the equations are up to 50% smaller than the maximum impact force obtained during the collision.

It this study, the impact forces are compared when the impact velocity is taken as 10 m/s in the AASHTO code suggested equations. This equivalent static impact force will be linearly decreased if a lower impact velocity is assumed. The indenter shape and impact location can have a significant influence on the impact force level as observed from the numerical simulations. These effects, however, are ignored in the code. It should also be noted that the numerical results obtained from the current study only address the head-on collision scenarios. For oblique impact accidents with an angle, the impact force should be reduced correspondingly with respect to the contact area.

In general, the code suggested equivalent static impact force can provide a reasonable reference in the early design phase. However, due to the uncertainties of impact location, impact angle, girder geometry and material type, it is recommended that these parameters should be taken into account in the detailed design phase or when the temporal evolvement of the impact force is of interest. Numerical simulations with both deformable deckhouse and girder models may be required to obtain more accurate force–deformation curves.

5. Analytical approach

As discussed in the above section, the deckhouse will suffer severe plastic deformations, while the girders undergo small damage and keeps essentially their shapes. Thus, the assumption of a rigid girder facilitates analytical prediction of the structural resistance of the deformable deckhouse using plastic methods [12,41].

5.1. Deformation mechanism

Based on the deckhouse deformation, the collision process can be simplified as a three-stage deformation mechanism as shown in Fig. 18 [42].

Stage 1: Plastic deformation develops in the front panel and the supporting stiffeners. Meanwhile, crushing deformation occurs in the vertical side panels. Local structural deformation occurs between two horizontal decks. For impact between two decks (Location 1), the total structural resistance for is obtained by adding up the membrane deformation of the front panel, the bending and membrane resistances of the attached stiffeners and the folding deformation of the side panels. For impact at the deck (Location 2), the crushing and bending resistance resistances of the impacted deck should also be included.

Stage 2: As the ship travels further, the upper and lower decks endure bending failure and the front panel in the upper and lower compartments are engaged. Rupture occurs in the front panel while the side

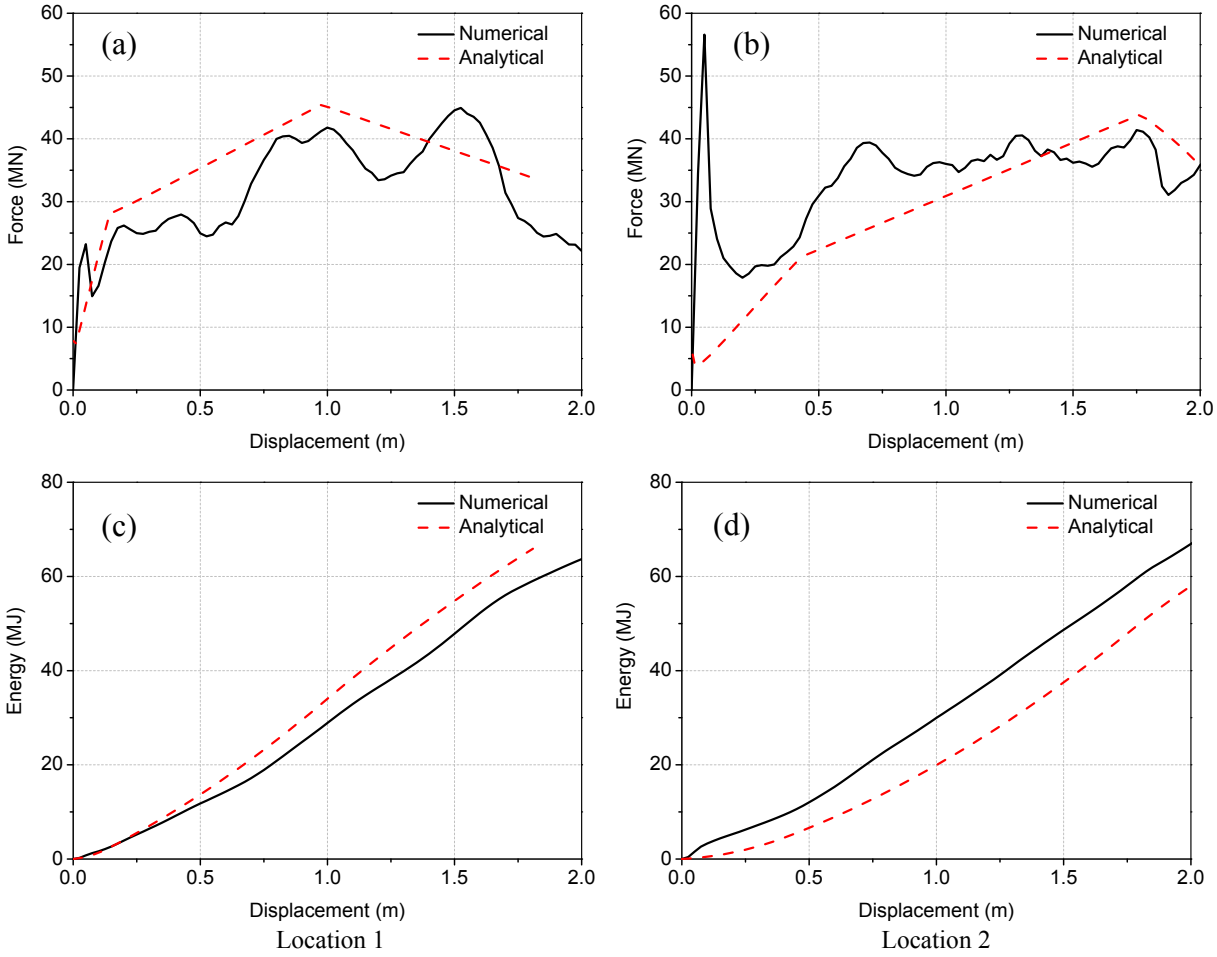

Fig. 22. Comparison between numerical and analytical results for collision with Girder 2. (a) Force at Location 1, (b) force at Location 2, (c) energy at Location 1, (d) energy at Location 2.

panels suffer continuous tearing after the first fold. The structural resistance in this stage includes the membrane deformation of the front panel, the bending and membrane resistances of the attached stiffeners, the folding and possible tearing of the vertical side panels. If the decks are strong, rupture may also initiate before the adjacent horizontal decks fail and lead to early loss of membrane forces in the front panel.

Stage 3: When the front plate is completely penetrated, the structural response is dominated by the crushing and bending resistances of the horizontal deck and the tearing of the vertical side plates.

5.2. Structural component response

The structural components of the deckhouse are assumed to behave independently, i.e., no coupling is considered [41,42]. Analytical formulae are developed for each structural component, and the total resistance and energy absorption are obtained by simply adding up the contributions of each individual structural component engaged in the collision [43]. Sha and Amdahl [42] calculated the impact resistance of a ship deckhouse subjected to rigid indenters by assembling the contributions of the front panel, the stiffeners, the side panels and the horizontal decks. It should be noted that the method was only proposed for deckhouse deformation under the impact of bridge girders with a sharp edge, e.g. Girder 1. The application is also limited to impact scenarios where the girder collides between two decks of the ship deckhouse, as shown in Fig. 19. The impact resistance of ship deckhouse subjected to sharp edge girder impact at the deck level and flat edge girder impacts was not considered in the study.

In this paper, the analytical method for prediction of deckhouse impact resistance is extended to cover the above collision scenarios. For sharp edge girder impact at the deck, the impact height L_1 and L_2 as shown in Fig. 19 should be taken as the height of a deck section, i.e. 2.6 m for the current deckhouse model. In addition, crushing and bending resistance resistances of the impacted deck should also be included.

When the deckhouse collides with flat edge girders, the membrane of the front panel in the ship deckhouse is developed in a reduced height compared with impacting with a sharp edge girder. Later, the deformation of the stiffened front panel and the side panels will also propagate earlier to the adjacent decks above and below the impact region. As more structural components will be involved in the collision process, higher impact resistance is expected. New deformation mechanisms for the front panel, the stiffeners and the side panel are developed as shown in Fig. 20.

5.3. Analytical derivation

Based on the proposed structural deformation mechanism, analytical equations can be used to calculate the resistance of each structural component with the following equations. The impact resistance of each structural component is described in Eqs. (4)-(10). For detailed derivations of the governing equations, it is referred to Sha and Amdahl [42].

The collision resistance of the front panel F_p and the supporting stiffeners F_s of the deckhouse are obtained by Eqs. (4) and (5) respectively.

$$F_p = \sigma_0 H_p t_p (\sin\alpha_1 + \sin\alpha_2) \tag{4}$$

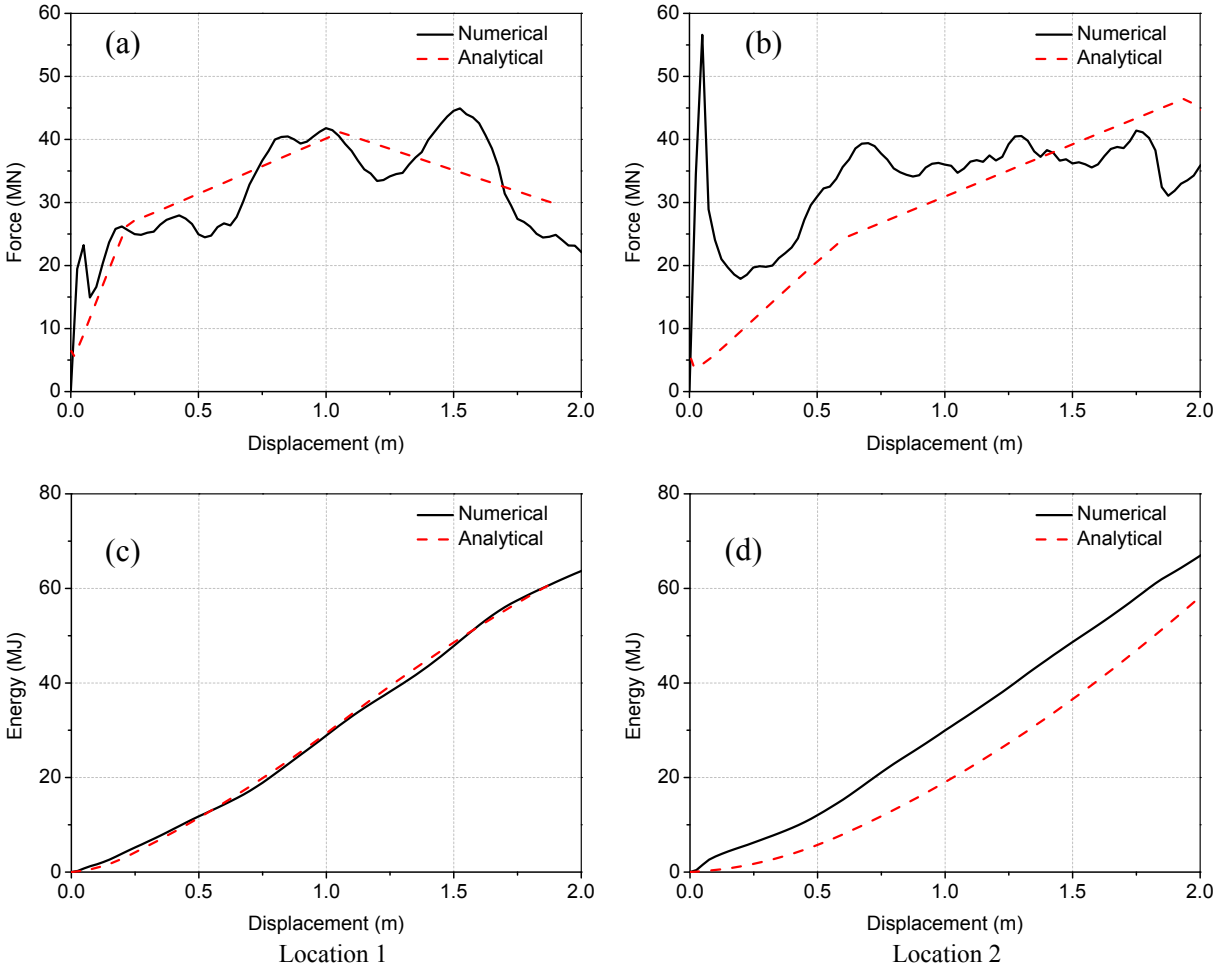

Fig. 23. Comparison between numerical and analytical results for collision with Girder 3. (a) Force at Location 1, (b) force at Location 2, (c) energy at Location 1, (d) energy at Location 2.

$$F_s = \frac{1}{2}\sigma_0 H_s t_s\left(\frac{\cos^2\alpha_1}{L_1}+\frac{\cos^2\alpha_2}{L_2}\right)+4\sigma_0 H_s t_s\left(\frac{\sin^2\alpha_1}{\cos^2\alpha_1 L_1}+\frac{\sin^2\alpha_2}{\cos^2\alpha_2 L_2}\right) \quad (5)$$

where σ_0 is the flow stress of steel. L_1 and L_2 are the distances to the top and bottom horizontal decks, respectively. h is the height of the girder flat edge. The corresponding rotational angles are α_1 and α_2, respectively. H_p and $t_p$are the width and thickness of the front panel, respectively. H_s and $t_s$are the width and thickness of the stiffeners and δ_p and δ_s are the deformation of the front panel and the attached stiffeners, respectively.

The folding resistance of the vertical side panels is calculated by [16]

$$F_g = 0.631\sigma_0 t_g^{1.83}\frac{L_1+L_2}{(L_1L_2)^{0.17}\delta_g^{0.5}}+0.645\sigma_0 t_g^{1.33}\delta_g\frac{L_1+L_2}{(L_1L_2)^{0.67}} \quad (6)$$

where t_g is the thickness of the side panel and δ_g is the deformation of the side panels. The folding length of the side panels H_g is obtained by

$$H_g = 0.8383\left(L_1L_2t_g\right)^{1/3} \quad (7)$$

After the fold, the tearing resistance of the side panels is expressed by [41]

$$F_w = 1.942\sigma_0 t_g^{1.5}\delta_g^{0.5}\varepsilon_m^{0.25}(tan\beta)^{0.5}\left(1+\frac{\mu}{tan\beta}\right) \quad (8)$$

where ε_m is the ultimate strain of the web girder [42], β is the half apex angle of the indenter and μ is the friction coefficient.

The horizontal decks still endure crushing and membrane failure regardless of the indenter shape. The crushing resistance F_{dc} and the membrane resistance of a horizontal deck F_{dm} are obtained by Eqs. (9) and (10) respectively [44].

$$F_{dc} = M_{d0}\frac{4}{R}(2C) \quad (9)$$

$$F_{dm} = \sigma_0 t_d H_d(\sin\gamma) \quad (10)$$

where M_{d0} represents the fully plastic bending moment capacity, R is the rolling radius and C is the breadth of the horizontal deck. γ is the rotational angle of the deck. H_d and $t_d$are the width and thickness of the horizontal decks, respectively.

5.4. Method validation

The impact resistance calculated by the proposed analytical method is compared with the force–displacement curves obtained from numerical simulations with rigid girders as shown in Figs. 21-23. In total, six collision scenarios with different girder shapes and impact locations are compared. It shows that the analytical method predicted impact force and energy dissipation (area under the force–displacement curve) agree quite well with the numerical simulation results for all scenarios. Both the development of the impact force and the fracture initiation and propagation are well captured. Hence, it may be conveniently used in

the preliminary design phases. The detailed procedure for the proposed method is described in [42]. An example is also provided in the referred study. It should be noted that the total energy in collision event is normally dissipated in two parts, i.e. local strain energy and global motion. This analytical approach only intends to estimate the impact force and the local strain energy dissipation.

6. Conclusions

In this paper, ship deckhouse-bridge girder collisions were numerically investigated with high-fidelity finite element models. The impact demand, energy dissipation and structural damage were obtained through a series of numerical simulations. The following conclusions are made:

1. Different vertical locations of impact on the deckhouse yield large variations of the collision force, depending on whether the horizontal decks in the ship deckhouse are involved in the deformation or not. This is not considered by the equivalent forces suggested by the AASHTO formulae or Pedersen's design chart. The cross-sectional shape (wedge or trapezoidal prism) of the bridge girder has a clear influence on the collision response when impacting between two decks. However, it does not have a significant effect on the collision response when the impact on the deck level is considered.
2. For the considered bridge girders and ship deckhouse, the resistance of the deckhouses is generally smaller than that of the bridge girder. Most of the collision energy is dissipated through the deformation of the ship deckhouse. However, the structural configuration of the bridge girders has a clear influence on the force–displacement curve.
3. As the simulations showed that the deckhouse damage was dominant during the collision process, a rigid girder assumption is thus justified. Assuming bridge girders to be rigid yields reasonably good estimations of the impact force and the structural damage in the deckhouse. However, the simplified rigid girders must be established based on the effective shape of the bridge girders, i.e. excluding the weak components, such as wind vanes.
4. An existing analytical approach for prediction of deckhouse resistance to penetration was extended to account for varying girder shape and impact location. Given the relatively small variation of ship deckhouse configurations, it is believed that this method can be widely applied in the preliminary design phase of a bridge.
5. The AASHTO code yields realistic impact forces, in the sense that the average force levels agree well with the simulations. However, the maximum force obtained is underpredicted by up to 50%. Due to the uncertainties of impact location, impact angle, girder geometry and material, it is recommended that these parameters should be taken into account in the detailed design phase or when the temporal evolvement of the impact force is of interest. Numerical simulations with both deformable deckhouse and girder models may be required to obtain more accurate force–deformation curves.

CRediT authorship contribution statement

Yanyan Sha: Conceptualization, Methodology, Writing - original draft. **Jørgen Amdahl:** Funding acquisition, Writing - review & editing. **Cato Dørum:** Funding acquisition, Writing - review & editing.

Declaration of Competing Interest

The authors declared that there is no conflict of interest.

Acknowledgements

This work is supported by the Norwegian Public Roads Administration under project number OF-10680 and OF-10753. The simulations were performed on resources provided by UNINETT Sigma2 - the National Infrastructure for High Performance Computing and Data Storage in Norway (project number NN9721K). These supports are gratefully acknowledged by the authors. The authors would also like to thank Dr Martin Storheim for providing the finite element model of the ship.

References

[1] Consolazio GR, Cowan DR. Nonlinear analysis of barge crush behavior and its relationship to impact resistant bridge design. Comput Struct 2003;81:547–57.
[2] Consolazio GR, Cowan DR. Numerically efficient dynamic analysis of barge collisions with bridge piers. J Struct Eng 2005;131:1256–66.
[3] Cowan DR, Consolazio GR, Davidson MT. Response-spectrum analysis for barge impacts on bridge structures. J Bridge Eng 2015;20:04015017.
[4] Fan W, Liu Y, Liu B, Guo W. Dynamic Ship-Impact Load on Bridge Structures Emphasizing Shock Spectrum Approximation. J Bridge Eng 2016;21:04016057.
[5] Fan W, Yuan W. Numerical simulation and analytical modeling of pile-supported structures subjected to ship collisions including soil–structure interaction. Ocean Eng 2014;91:11–27.
[6] Fan W, Yuan W, Yang Z, Fan Q. Dynamic demand of bridge structure subjected to vessel impact using simplified interaction model. J Bridge Eng 2010;16:117–26.
[7] Sha Y, Amdahl J. Numerical investigations of a prestressed pontoon wall subjected to ship collision loads. Ocean Eng 2019;172:234–44.
[8] Sha Y, Hao H. Nonlinear finite element analysis of barge collision with a single bridge pier. Eng Struct 2012;41:63–76.
[9] Sha Y, Hao H. Laboratory tests and numerical simulations of barge impact on circular reinforced concrete piers. Eng Struct 2013;46:593–605.
[10] Wang W, Morgenthal G. Dynamic analyses of square RC pier column subjected to barge impact using efficient models. Eng Struct 2017;151:20–32.
[11] Yuan P, Harik IE. Equivalent barge and flotilla impact forces on bridge piers. J Bridge Eng 2009;15:523–32.
[12] Sha Y, amdahl J, Liu K. Design of steel bridge girders against ship forecastle collisions. Engineering Structures. 2019.
[13] Press TA. 2012.
[14] Mainichi T. 2018.
[15] Minorsky V. An analysis of ship collisions with reference to protection of nuclear power plants. Sharp (George G.) Inc., New York; 1958.
[16] Zhang S. The mechanics of ship collisions: Institute of Naval Architecture and Offshore. Engineering 1999.
[17] Woisin G. Design against collision. GKSS-Forschungszentrum 1980.
[18] Svensson H. Protection of bridge piers against ship collision. Steel Construction. 2009;2:21–32.
[19] Consolazio GR, Cook RA, McVay MC, Cowan D, Biggs A, Bui L. Barge impact testing of the St. George Island causeway bridge: Department of Civil and Coastal Engineering, University of Florida; 2006.
[20] Liu B, Soares CG. Assessment of the strength of double-hull tanker side structures in minor ship collisions. Eng Struct 2016;120:1–12.
[21] Pedersen PT, Valsgaard S, Olsen D, Spangenberg S. Ship impacts: bow collisions. Int J Impact Eng 1993;13:163–87.
[22] Servis D, Samuelides M, Louka T, Voudouris G. Implementation of finite-element codes for the simulation of ship-ship collisions. Journal of ship research. 2002;46:239–47.
[23] Amdahl J. Energy absorption in ship-platform impacts. 1983.
[24] Moan T, Amdahl J, Ersdal G. Assessment of ship impact risk to offshore structures-New NORSOK N-003 guidelines. Mar struct 2017.
[25] Storheim M, Amdahl J. Design of offshore structures against accidental ship collisions. Mar struct 2014;37:135–72.
[26] Travanca J, Hao H. Numerical analysis of steel tubular member response to ship bow impacts. Int J Impact Eng 2014;64:101–21.
[27] Kang L, Magoshi K, Ge H, Nonaka T. Accumulative response of large offshore steel bridge under severe earthquake and ship impact due to earthquake-induced tsunami flow. Eng Struct 2017;134:190–204.
[28] Fan W, Shen D, Huang X, Sun Y. Reinforced concrete bridge structures under barge impacts: FE modeling, dynamic behaviors, and UHPFRC-based strengthening. Ocean Eng 2020;216. 108116.
[29] Fan W, Sun Y, Yang C, Sun W, He Y. Assessing the response and fragility of concrete bridges under multi-hazard effect of vessel impact and corrosion. Eng Struct 2020;225. 111279.
[30] Fan W, Zhang Z, Huang X, Sun W. A simplified method to efficiently design steel fenders subjected to vessel head-on collisions. Mar struct 2020;74. 102840.
[31] Sha Y, Amdahl J, Dørum C. Local and global responses of a floating bridge under ship-girder collisions. J Offshore Mech Arct Eng 2018.
[32] Vrouwenvelder A. Design for ship impact according to Eurocode 1, Part 2. 7. Ship collision analysis. 1998,:123–34.
[33] AASHTO. Guide Specification and Commentary for vessel collision design of highway bridges. Washington, DC: American Association of State Highway and Transportation Officials; 1991.
[34] Larsen OD. Ship collision with bridges: The interaction between vessel traffic and bridge structures. IABSE 1993.
[35] Sha Y, Amdahl J. Ship Collision Analysis of a Floating Bridge in Ferry-Free E39 Project. 36th International Conference on Ocean, Offshore and Arctic Engineering: American Society of Mechanical Engineers; 2017. p. V009T12A21.
[36] Alsos HS, Amdahl J, Hopperstad OS. On the resistance to penetration of stiffened plates, Part II: Numerical analysis. Int J Impact Eng 2009;36:875–87.

[37] Fan W, Xu X, Zhang Z, Shao X. Performance and sensitivity analysis of UHPFRC-strengthened bridge columns subjected to vehicle collisions. Eng Struct 2018;173:251–68.
[38] Sha Y, Hao H. Laboratory tests and numerical simulations of CFRP strengthened RC pier subjected to barge impact load. Int J Struct Stab Dyn 2015;15. 1450037.
[39] Paik JK, Pedersen PT. Modelling of the internal mechanics in ship collisions. Ocean Eng 1996;23:107–42.
[40] Storheim M, Amdahl J. On the sensitivity to work hardening and strain-rate effects in nonlinear FEM analysis of ship collisions. Ships and Offshore Structures. 2017;12:100–15.
[41] Sun B, Hu Z, Wang G. An analytical method for predicting the ship side structure response in raked bow collisions. Mar struct 2015;41:288–311.
[42] Sha Y, Amdahl J. A simplified analytical method for predictions of ship deckhouse collision loads on steel bridge girders. Ships Offshore Structures. 2018:1–14.
[43] Pedersen PT. Review and application of ship collision and grounding analysis procedures. Mar struct 2010;23:241–62.
[44] Hong L, Amdahl J. Rapid assessment of ship grounding over large contact surfaces. Ships Offshore Struct. 2012;7:5–19.